AIAA JOURNAL
Vol. 35, No. 12, December 1997

Semiactive Vibration Suppression with Electrorheological-Fluid Dampers

Junjiro Onoda*
Institute of Space and Astronautical Science, Sagamihara, Kanagawa 229, Japan
Hyun-Ung Oh†
University of Tokyo, Bunkyo-ku, Tokyo 113, Japan
and
Kenji Minesugi‡
Institute of Space and Astronautical Science, Sagamihara, Kanagawa 229, Japan

Semiactive vibration suppression with electrorheological (ER)-fluid variable dampers is proposed and demonstrated to be a robust approach to suppressing the vibration of space structures. The principal characteristics of an ER-fluid variable damper are measured, and a simple mathematical model of the damper is proposed. Based on the mathematical model of the damper, several semiactive on–off control laws are proposed. Their performance is investigated through both numerical simulations and experiments of cantilevered truss beams with ER-fluid variable dampers. Simulation results indicate that most of the proposed laws result in much more effective vibration suppression than is obtained when using an optimally tuned passive system. Under an ill condition, they are also shown to be much more robust than linear quadratic Gaussian active vibration controls whose vibration suppression performance is almost the same. A semiactive vibration suppression experiment with a cantilevered 10-bay truss beam demonstrates that vibrations are suppressed effectively by the ER-fluid variable damper.

I. Introduction

ACTIVE vibration suppression is a very attractive and powerful approach to suppressing the vibration of space structures.[1] Although many works on robust control logic have been published, the technology is still experiencing problems with instability due to phenomena such as spillover,[2] especially when the exact dynamic characteristics of the structures are not known. On the other hand, passive systems, whose vibration energy is dissipated by structural damping, viscosity, friction, etc., are always stable. Although this robustness is a great advantage, passive systems usually have disadvantages with regard to their damping performance. One attractive approach to making passive damping systems less disadvantageous is semiactive vibration suppression, or controlling the states of systems such that their inherent damping performances are enhanced. Because the semiactive approach suppresses vibration by exploiting passive energy dissipation mechanisms, systems are stable even when the control logic is improper as a result of the lack of exact information about the dynamic characteristics of the structures. Space structural systems are required to be extremely reliable, but it is very difficult to predict the dynamic characteristics of space structures that are deployed or constructed in orbit. The robust semiactive approaches, therefore, seem to be especially suitable for space structures.

Several types of semiactive vibration suppression have been proposed and studied. For space truss structures, Onoda et al.[3] and Onoda and Minesugi[4] proposed and investigated vibration suppression by stiffness control using hysteretic variable-stiffness members. They also proposed to control the friction of variable-friction devices for semiactive vibration suppression of truss structures[5] and tension-stabilized structures.[6] Semiactive vibration suppression of truss structures by dashpot-type variable-viscosity dampers has also been proposed and investigated.[7]

To implement passive or semiactive vibration suppression, many researchers have been interested in electrorheological (ER) fluids, whose damping characteristics vary according to the strength of an applied electric field.[8] Many studies on the semiactive approaches with ER fluid have been reported. Stanway et al.[9] fabricated a variable damper with ER fluid and investigated its characteristics. They concluded that its characteristics can be roughly represented by viscous plus coulomb friction, although it is very complicated. Gavin et al.[10] also measured and modeled detailed characteristics of ER-fluid dampers. Wang et al.[11] proposed and demonstrated a sliding-mode control scheme for semiactive suppression of single-mode vibration with an ER-fluid variable damper. For a beam containing ER fluid, a simpler semiactive control scheme has been proposed and demonstrated by Choi and Park.[12] Onoda et al.[13] also fabricated an ER-fluid damper and performed preliminary analytical and experimental studies of semiactive vibration suppression with it.

This paper, an extension of the preliminary study in Ref. 13, first describes a variable damper with ER fluid, the characteristics of the damper, and a simple mathematical model of the damper. Next, based on the simple mathematical model of the damper, several control laws for multiple-degree-of-freedom structures with multiple dampers are proposed and evaluated by numerical simulations. Finally, an experiment demonstrates the effectiveness of the scheme for the suppression of multiple-mode vibration of an actual structure.

II. ER-Fluid Variable Damper

As shown in Fig. 1, the ER-fluid damper[13] studied consists of two variable-volume chambers filled with ER fluid and a bottleneck connecting them. The damper is sealed with bellows, and the ER fluid is pressurized by a spring so that it can be used in the vacuum of a space environment. The characteristics of the ER fluid in the bottleneck vary according to the voltage applied to the electrode, thus varying the characteristics of the damper. Because the purpose of the study is simply to evaluate and demonstrate the concept of semiactive vibration suppression with the ER-fluid damper, weight saving is not a consideration in the design and fabrication of this damper. Some key dimensions are shown in Fig. 1.

The ER fluid used is Bridgestone NS-6, which is a commercially available fluid consisting of carbonaceous particles in silicone oil. To reduce $f_{\min}$ (which will be defined later), the top fluid from partially precipitated ER fluid is intentionally used in the following

Received Dec. 11, 1996; revision received May 17, 1997; accepted for publication July 29, 1997.

*Professor, Research Division for Space Transportation, 3-1-1, Yoshinodai. Member AIAA.
†Graduate Student, Department of Aeronautics and Astronautics, 731, Hongo.
‡Associate Professor, Research Division for Space Transportation, 3-1-1, Yoshinodai. Member AIAA.

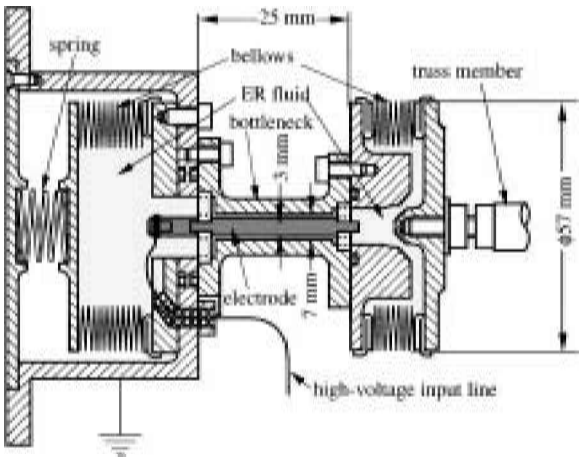

Fig. 1 Construction of ER-fluid variable damper.

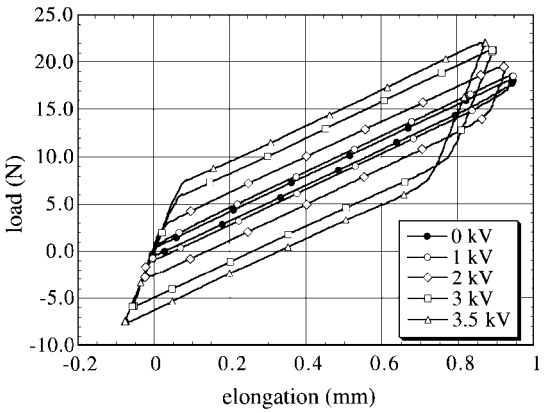

Fig. 2 Load-extension relation measured in extension/contraction tests; extension rate = 20 mm/min.

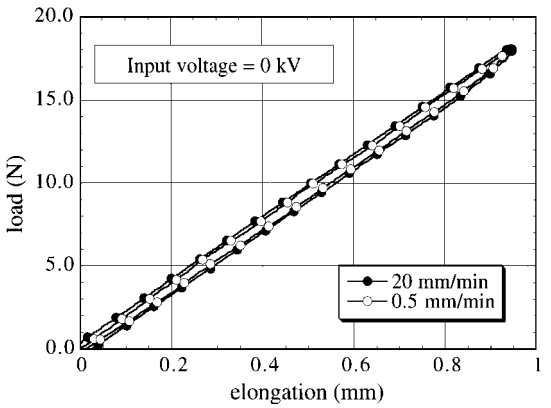

Fig. 3 Effect of extension/contraction rate on the load-elongation relation; 0-kV input, extension rate = 20 and 0.5 mm/min.

tests. Therefore, the concentration of solid in the ER fluid is less than that in the original NS-6.

To measure the characteristics of the damper, several constant-rate extension tests were performed while keeping the input voltage constant. Figure 2 shows the elongation-load relation measured while repeating the constant-rate extension and contraction at various constant input voltages. Figure 2 shows that the higher the input voltage is, the larger the hysteresis is. The plot obtained at each input voltage consists of high-stiffness and low-stiffness sections forming a parallelogram. Each stiffness is almost the same as that obtained at another input voltage. Figure 3 shows the elongation-load relation measured in extension/contraction tests at two extension/contraction rates when no voltage is applied. Figure 3 shows that the effect of the extension/contraction rate is small in this case.

Using these data, we can model the damper with two spring elements k_1 and k_2, a viscous damping element c, and a variable

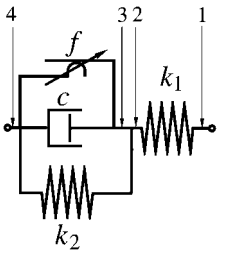

Fig. 4 Mathematical model of an ER-fluid variable damper.

coulomb frictional element f (Fig. 4). This model is consistent with the Bingham fluid characteristics of ER fluid and with the structure of the damper. Spring constant k_1 seems to be dominated by the volume stiffness of the fluid and the chamber, and k_2 seems to be dominated by the axial stiffness of the bellows. Because k_1 and $k_1k_2/(k_1+k_2)$ correspond, respectively, to the stiffnesses in the high-stiffness and low-stiffness ranges of Fig. 2, the values of k_1 and k_2 can be estimated as 1.00–1.02×10^5 N/m and 2.2–2.3×10^4 N/m, respectively, which are almost independent from the input voltage.

The value of c may be too small to be accurately estimated from the extension/contraction test results, but from Fig. 3 we can see that it is less than 1×10^3 N s/m. Although the values of c may be dependent on the input voltage, its effect on the following semiactive vibration suppression is negligible because, as shown later, the extension/contraction rate of the viscous element is almost always zero when a high voltage is applied in the following vibration suppression scheme. Therefore, it is assumed in this investigation to be constant.

From the elongation-load relation obtained in the constant-rate extension tests, the value of f is estimated as

$$f = (k_1 + k_2)(p_1 - p_2)/(2k_1) - c|\dot{d}| \tag{1}$$

where p_1 and p_2 are the loads at a certain value of elongation in the low-stiffness range in the extension and contraction processes, respectively, and $\dot{d}$ is the extension/contraction rate. The value of c is assumed to be 1×10^3 N s/m in both cases. Although this assumption may result in some underestimation of f, the amount of this underestimation is less than 0.3 N. The estimated value of f for 0-, 1-, 2-, 3-, and 3.5-kV input voltages are approximately 0.2, 0.7, 2.7, 5.4, and 7.0 N, respectively. The value of f is roughly proportional to the square of the input voltage rather than the input voltage. This trend is consistent with Ref. 10 but conflicts with Ref. 9, whose authors concluded that the input voltage has a much greater effect on viscosity than it does on coulomb friction. As shown later, the semiactive control in this paper is limited to the on–off type. Therefore, only the values of $f_{\max}$ and $f_{\min}$ are related to the vibration suppression performance, where $f_{\max}$ and $f_{\min}$ are the values of f at the maximum and minimum input voltages $V_{\max}$ and $V_{\min}$, respectively. The measurement of detailed relation between f and the input voltage V is out of the scope of this paper. Although no data are shown, both the ER-fluid damper and the high-voltage amplifier used in this experiment were confirmed to respond to the input voltage quickly, within a few milliseconds.

In this discussion, the parameter values such as k_1, k_2, c, and f have been estimated for the present particular damper. However, it is clear that the parameter values can be adjusted by selecting proper dimensional sizes and ER fluid.

III. Equations of Motion

We investigate truss structures with ER-fluid variable dampers, which are modeled as shown in Fig. 4. The equations of motion of the structures are written in the physical coordinates as

$$M\ddot{\boldsymbol{x}} + C\dot{\boldsymbol{x}} + K\boldsymbol{x} + HD\boldsymbol{e} = \boldsymbol{w} \tag{2}$$

$$\begin{aligned} \dot{e}_i &= \frac{p_i - k_{2i}e_i - f_i}{c_i} && \text{when} \quad p_i - k_{2i}e_i > f_i \\ \dot{e}_i &= 0 && \text{when} \quad -f_i \le p_i - k_{2i}e_i \le f_i \\ \dot{e}_i &= \frac{p_i - k_{2i}e_i + f_i}{c_i} && \text{when} \quad p_i - k_{2i}e_i < -f_i \end{aligned} \tag{3}$$

$$\boldsymbol{p} = -D(H^T\boldsymbol{x} + \boldsymbol{e}) \tag{4}$$

where

$$D = \mathrm{diag}\left[\frac{k_{1i}(EA_i/l_i)}{k_{1i} + (EA_i/l_i)}\right] \tag{5}$$

and where $\boldsymbol{x}$ is the displacement vector; M is the mass matrix; C is the damping matrix; K is the stiffness matrix of the truss whose frictional elements of dampers are all stuck, i.e., under the condition of $e_i = 0$; EA_i and l_i are the axial stiffness and the length of the truss member connected to the ith variable damper, respectively; H is a matrix composed of directional cosines of the truss members with the variable dampers; $\boldsymbol{w}$ is the external force vector; $\boldsymbol{e}$ is a vector composed of e_i; e_i is the elongation between points 2 and 4 in Fig. 4; $\boldsymbol{p}$ is a vector composed of p_i; p_i is the tensile load on the damper; the subscript i $(i = 1, 2, \ldots, n_d)$ denotes the ith variable damper; and n_d is the number of ER-fluid variable dampers.

If we assume a damping ratio ζ for each mode, Eqs. (2) and (4) can be written in the modal coordinates as

$$\ddot{\boldsymbol{q}} + 2\zeta\Omega^{\frac{1}{2}}\dot{\boldsymbol{q}} + \Omega\boldsymbol{q} + \Phi^T H D\boldsymbol{e} = \Phi^T\boldsymbol{w} \tag{6}$$

$$\boldsymbol{p} = -D(H^T\Phi\boldsymbol{q} + \boldsymbol{e}) \tag{7}$$

where $\boldsymbol{q}$ is the modal displacement vector; Ω and $\Omega^{1/2}$ are diagonal matrices composed of ω_i^2 and ω_i, respectively; ω_i^2 is the ith eigenvalue; Φ is a matrix composed of eigenvectors normalized such that

$$\Phi^T M\Phi = I \tag{8}$$

and I is a unit matrix of a proper size.

IV. Semiactive Control Laws

For ease of practical implementation, we assume that the values of f_i are limited to either $f_{\max}$ or $f_{\min}$ $(0 \le f_{\min} < f_{\max})$, corresponding to the maximum and minimum input voltages $V_{\max}$ and $V_{\min}$, respectively. In other words, the present investigation is limited to on–off controls.

Maximum Load Friction Control (MLFC)

When the values of c and $f_{\min}$ are zero and $f_{\max}$ is infinitely large, the present system becomes identical to the variable stiffness system studied in Refs. 3 and 4. When the value of $f_{\min}$ is zero and $f_{\max}$ is infinitely large, the present system becomes identical with an extreme case of the variable damping system[7] whose upper limit of c is infinitely large. Therefore, by analogy with control logic C of Ref. 3 and maximum load damping control (MLDC) of Ref. 7, a possible on–off control scheme is as follows: minimize f_i when $|p_i|$ is at a maximum, and subsequently maximize f_i when $|p_i|$ ceases decreasing. This control law is simple and suitable for distributed control because only locally available information is required for the control of each variable damper. In this paper, this control law is referred to as MLFC.

Linear Quadratic Friction Control-1 (LQFC-1)

When the external force is absent, Eq. (6) can be written as

$$\dot{\boldsymbol{z}}_1 = A_1\boldsymbol{z}_1 + B_1\boldsymbol{e} \tag{9}$$

where

$$\boldsymbol{z}_1 = \lfloor \boldsymbol{q}^T, \dot{\boldsymbol{q}}^T \rfloor^T \tag{10}$$

$$A_1 = \begin{bmatrix} 0 & I \\ -\Omega & -2\zeta\Omega^{\frac{1}{2}} \end{bmatrix} \tag{11}$$

and

$$B_1 = \begin{bmatrix} 0 \\ -\Phi^T H D \end{bmatrix} \tag{12}$$

If we could directly control the value of $\boldsymbol{e}$, we could use any linear control logic based on Eq. (9). For example, the linear quadratic regulator (LQR) control theory[14] tells us that the optimal control that minimizes

$$J \equiv \int_0^\infty \left(\boldsymbol{z}_1^T R_1\boldsymbol{z}_1 + \boldsymbol{e}^T R_2\boldsymbol{e}\right) \mathrm{d}t \tag{13}$$

for given weighting matrices R_1 and R_2 is given as

$$\boldsymbol{e} = \boldsymbol{e}_T \equiv -F_1\boldsymbol{z}_1 \tag{14}$$

where F_1 is the gain matrix given as

$$F_1 = R_2^{-1}B_1^T P_1 \tag{15}$$

and P_1 is the positive definite solution of the following Riccati equation:

$$P_1B_1R_2^{-1}B_1^T P_1 - A_1^T P_1 - P_1A_1 - R_1 = 0 \tag{16}$$

In the present system, however, we cannot control the value of $\boldsymbol{e}$ directly. Therefore, let us control f_i such that each element of $\boldsymbol{e}$ traces the corresponding element of $\boldsymbol{e}_T$ as faithfully as possible. What we can do is prevent the variation of e_i by increasing f_i when e_i is about to vary away from e_{Ti} and promote the variation by decreasing f_i when e_i is expected to vary toward e_{Ti}. Because Eq. (3) indicates that the sign of $\dot{e}_i$ is the same as that of $p_i - k_{2i}e_i$ when $\dot{e}_i \ne 0$, a possible control logic for this scheme is

$$\begin{aligned} f_i &= f_{\min} \quad \text{when} \quad (p_i - k_{2i}e_i)(e_{Ti} - e_i) > 0 \\ f_i &= f_{\max} \quad \text{when} \quad (p_i - k_{2i}e_i)(e_{Ti} - e_i) < 0 \end{aligned} \tag{17}$$

In this paper, this control law is referred to as linear quadratic friction control-1-a (LQFC-1-a).

In the LQR control, a large value of $\boldsymbol{e}$ is penalized, as shown in Eq. (13). In the present system, however, large value of $\boldsymbol{e}$ does not require large energy, and it is not necessary to penalize it. Therefore, better performance may be obtained by controlling f_i such that the absolute value of e_i becomes maximum when the sign of e_i is the same as that of e_{Ti} and such that it becomes minimum otherwise. This strategy can be implemented by the following control law, which is called LQFC-1-b:

$$\begin{aligned} f_i &= f_{\min} \quad \text{when} \quad (p_i - k_{2i}e_i)e_{Ti} > 0 \\ f_i &= f_{\max} \quad \text{when} \quad (p_i - k_{2i}e_i)e_{Ti} < 0 \end{aligned} \tag{18}$$

LQFC-2

When the external force is absent, Eqs. (3) and (6) can be combined and rewritten as

$$\dot{\boldsymbol{z}}_2 = A_2\boldsymbol{z}_2 + B_2\boldsymbol{v} \tag{19}$$

where

$$\boldsymbol{z}_2 = \lfloor \boldsymbol{q}^T, \dot{\boldsymbol{q}}^T, \boldsymbol{e}^T \rfloor^T \tag{20}$$

$$A_2 = \begin{bmatrix} 0 & I & 0 \\ -\Omega & -2\zeta\Omega^{\frac{1}{2}} & \Phi^T H D \\ 0 & 0 & 0 \end{bmatrix} \tag{21}$$

$$B_2 = \begin{bmatrix} 0 \\ 0 \\ I \end{bmatrix} \tag{22}$$

and

$$\begin{aligned} v_i &= \frac{p_i - k_{2i}e_i - f_i}{c_i} \quad \text{when} \quad p_i - k_{2i}e_i > f_i \\ v_i &= 0 \quad \text{when} \quad -f_i \le p_i - k_{2i}e_i \le f_i \\ v_i &= \frac{p_i - k_{2i}e_i + f_i}{c_i} \quad \text{when} \quad p_i - k_{2i}e_i < -f_i \end{aligned} \tag{23}$$

If we could directly control the value of $\boldsymbol{v}$ without any limitation, the LQR control logic tells us that $\boldsymbol{v}$ should be controlled such that

$$\boldsymbol{v} = \boldsymbol{v}_T \equiv -F_2\boldsymbol{z}_2 \tag{24}$$

where F_2 is the gain matrix given by the LQR theory. This differs from the preceding case in that we can directly control $\boldsymbol{v}$ by controlling $\boldsymbol{f}$. However, the value of f_i is limited to either $f_{\max}$ or $f_{\min}$.

Therefore, a possible strategy, similar to LQFC-1, is to select the value of f_i that gives a value of v_i closer to v_{Ti} than the other value does, where v_{Ti} is the ith element of vector $\boldsymbol{v}_T$. This strategy can be implemented by

$$\begin{aligned} f_i &= f_{\min} \qquad \text{when} \qquad (v_{Ti} - v_{Ai})(v_{Ni} - v_{Ai}) > 0 \\ f_i &= f_{\max} \qquad \text{when} \qquad (v_{Ti} - v_{Ai})(v_{Ni} - v_{Ai}) < 0 \end{aligned} \tag{25}$$

where v_{Ni} is the value of v_i given by $f_{\min}$, v_{Xi} is the value of v_i given by $f_{\max}$, and v_{Ai} is an average of v_{Ni} and v_{Xi}. This control law is called LQFC-2-a.

In this case also, there is no cost for a large value of v_i. Therefore, another possible approach, similar to LQFC-1-b, is to make the absolute value of v_i maximum when the polarities of v_i and v_{Ti} are identical and to make the absolute value of v_i minimum otherwise. Because Eq. (23) indicates that the polarity of v_i is identical with that of $p_i - k_{2i}e_i$ when $v_i \neq 0$, this strategy can be implemented by the following control law:

$$\begin{aligned} f_i &= f_{\min} \qquad \text{when} \qquad v_{Ti}(p_i - k_{2i}e_i) > 0 \\ f_i &= f_{\max} \qquad \text{when} \qquad v_{Ti}(p_i - k_{2i}e_i) < 0 \end{aligned} \tag{26}$$

This control law is called LQFC-2-b.

Observer

To actually implement LQFC control laws, modal displacements and velocities have to be estimated from some measured data. A standard scheme for estimating them is to use the following observer, which is often used for active control in combination with LQR:

$$\dot{\hat{\boldsymbol{z}}}_1 = A_1\hat{\boldsymbol{z}}_1 + B_1\boldsymbol{e} + K_O(\boldsymbol{y} - C_1\hat{\boldsymbol{z}}_1) \tag{27}$$

where $\hat{\boldsymbol{z}}_1$ is the estimated value of $\boldsymbol{z}_1$, C_1 is the output matrix, and $\boldsymbol{y}$ is the output of the sensor. The output is a linear function of $\boldsymbol{z}_1$:

$$\boldsymbol{y} = C_1\boldsymbol{z}_1 \tag{28}$$

The observer gain K_O that minimizes the estimation error under a noisy condition is given[14] as

$$K_O = QC_1^T V_2^{-1} \tag{29}$$

where Q is the positive definite solution of

$$QC_1^T V_2^{-1} C_1 Q - AQ - QA^T - V_1 = 0 \tag{30}$$

and V_1 and V_2 are intensity matrices of the white noise disturbance to the structure and white noise in the sensor signal, respectively. Once $\hat{\boldsymbol{z}}_1$ is obtained, $\hat{\boldsymbol{z}}_2$ (the estimated value of $\boldsymbol{z}_2$) is obtained for LQFC-2 control laws from Eq. (20) when $\boldsymbol{e}$ is measured. When the observer is used, Eqs. (14) and (24) are rewritten as

$$\boldsymbol{e} = \boldsymbol{e}_T \equiv -F_1\hat{\boldsymbol{z}}_1 \tag{14'}$$

and

$$\boldsymbol{v} = \boldsymbol{v}_T \equiv -F_2\hat{\boldsymbol{z}}_2 \tag{24'}$$

V. Numerical Simulations and Discussions

To investigate the performances of the aforementioned semiactive schemes with ER-fluid variable dampers, we numerically investigate the vibration suppression of the cantilevered 10-bay truss beams shown in Figs. 5. This truss beam basically corresponds to the truss used for the experiment in Sec. VI. The total length of the truss beam is 3.8 m, a 2.7-kg mass is mounted at the tip, and a 1.0-kg mass is mounted at each of the four central nodes of the beam truss. The axial stiffness of the truss members are intentionally reduced by using plate springs to reduce the natural frequency of the structure so that a relatively slow processor could control it in the experiment, which will be described in Sec. VI. The axial stiffness of the longitudinal and lateral members is 1.48×10^4 N, and that of the diagonal members is 2.00×10^4 N. The mass of each longitudinal and lateral member is 82 g, and that of each diagonal member is 88 g. The mass of each node is 21 g. The k_1 and k_2 values of the damper are $k_1 = 1.05 \times 10^5$ N/m and $k_2 = 2.5 \times 10^4$ N/m, which are almost

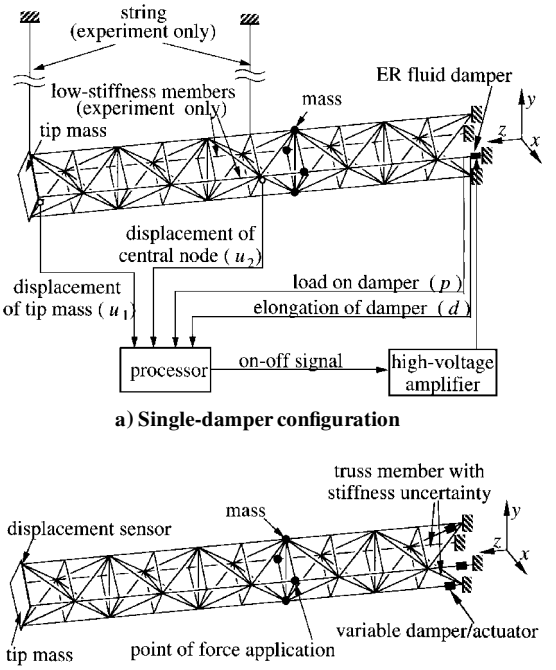

Fig. 5 Cantilevered 10-bay truss beam with variable dampers.

identical to the values measured in Sec. III. The damping ratio ζ is assumed to be 0.5%. The $f_{\max}$ of the dampers was assumed to be 10 N, and $f_{\min}$ was assumed to be zero unless otherwise noted. The damping performance was investigated for various values of c. In the following numerical simulations, the truss with an ER-fluid damper is first investigated to clarify the basic behavior, and then the vibration suppression of a truss with three ER-fluid dampers is investigated.

Vibration Suppression with a Single Damper

The semiactive vibration suppression of the truss shown in Fig. 5a was numerically simulated first. All of the vibration modes that were symmetric with respect to the x–z plane were taken into consideration in the simulation, but the other modes were not taken into account so that the system would be controllable. After the modal displacements of the first symmetric mode was set to 10 mm $\text{kg}^{1/2}$ and the modal displacements of all of the other modes were set to zero, the structure was freed, and subsequent vibration was suppressed by the ER-fluid damper with the aforementioned control laws. In LQFC-1 control laws, matrix R_1 was set as

$$R_1 = \text{diag}\left(1, 1, \ldots, 1, 1/\omega_1^2, 1/\omega_2^2, \ldots, 1/\omega_{n_c}^2\right) \tag{31}$$

and in LQFC-2 control laws, it was set as

$$R_1 = \text{diag}\left(1, 1, \ldots, 1, 1/\omega_1^2, 1/\omega_2^2, \ldots, 1/\omega_{n_c}^2, 0\right) \tag{32}$$

where n_c is the number of controlled modes. In both the LQFC-1 and LQFC-2 control laws, R_2 was set as

$$R_2 = r_2 I \tag{33}$$

where r_2 is a constant scalar. For LQFC-1-a, LQFC-1-b, LQFC-2-a, and LQFC-2-b, the values of r_2 were set as 1×10^4 kg, 1×10^6 kg, 10 kg s^2, and 100 kg s^2, respectively. These values roughly minimized

$$I_{\text{rms}} = \int_0^{\tau_I} \delta_{\text{rms}}\, \text{d}t \tag{34}$$

throughout a large range of the value of c of the damper, where δ_{rms} is the root mean square of displacements of all of the truss nodes and $\tau_I = 10$ s. The lowest two modes were taken into the account to design the LQFC control laws, i.e., $n_c = 2$. In this investigation with single-damper configuration, the observer was not used and the state vector was assumed to be known.

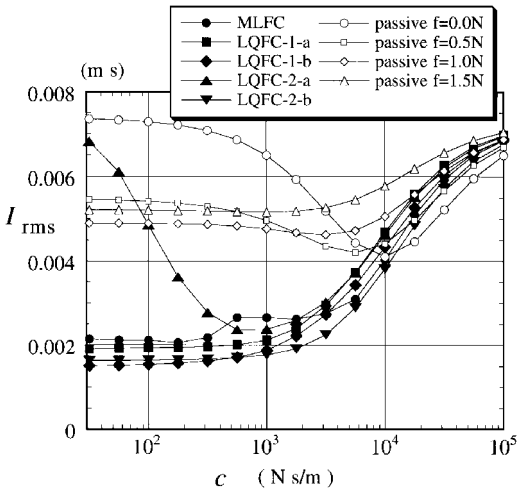

Fig. 6 Value of I_{rms} from various semiactive control laws and from passive systems with various levels of frictional force; single damper, only the first mode is excited by the initial condition.

Equations of motion in the modal coordinates were numerically integrated using the Runge–Kutta scheme with the double-precision option. The time step size for the integration was 1×10^{-4} s, which is much smaller than the vibration period of the highest mode (7.4×10^{-3} s). When the value of c of the damper was 32 N s/m, which is the minimum value in the following investigation, the time constant of the damper, $c/(k_1 + k_2)$, became minimum and was 2.5×10^{-4} s. Even at this value of c, however, the difference between the value of I_{rms} obtained from the numerical simulation with the time step size of 1×10^{-4} s and the value obtained with the time step size of 2×10^{-5} s was less than 0.32% in all of the cases other than MLFC, and it was less than 3.2% in the MLFC case. Therefore, the following numerical simulation results seem to be accurate enough for the present discussion.

Figure 6 shows the values of I_{rms} obtained from the various control laws. Figure 6 also shows the values from the passive system, whose f and c are constant. The passive system is optimal, i.e., I_{rms} from the passive system is minimum, when $c = 1 \times 10^4$ N s/m and $f = 0$. The values of I_{rms} from MLFC, LQFC-1-a, LQFC-1-b, and LQFC-2-b control laws are 36–65% of that of the optimally tuned passive system when c is less than approximately 1×10^3 N s/m. The value obtained from LQFC-2-a is about 58% of that of optimal passive system when the value of c is in the range of 5×10^2–1×10^3 N s/m. Because smaller value of I_{rms} indicates higher damping performance, these facts indicate that the damping performances of the semiactive systems are much better than that of the optimally tuned passive system and that these semiactive approaches are effective if the value of c is designed properly. Figure 6 also shows that the performances of semiactive approaches except for LQFC-2-a are less sensitive to the variation of c than the optimal passive system is.

Figure 7 shows time histories obtained from LQFC-1-b with $c = 1 \times 10^3$ N s/m. E_s denotes the energy stored in the damper and the truss member on which the damper is installed, and E_d denotes the cumulative energy dissipated by the damper. The value of e is indirectly controlled such that its absolute value becomes maximum when its polarity is the same as e_T and is otherwise minimum, just as the LQFC-1-b control law intends. In the initial phase, the value of f is decreased at (or near) the peaks of the first modal displacement or at the peak of E_s. When f is decreased, e varies stepwise, dissipating energy effectively. As a result, E_s decreases stepwise and E_d increases stepwise. The first-mode vibration is, consequently, suppressed nicely. The second mode is excited by the control action, but its amplitude is small and it damps out gradually. The time history of f indicates that the control is devoted to the suppression of the first-mode vibration before $t = 3$ s. After $t = 8$ s, however, when the first-mode vibration has been suppressed, it is devoted to the suppression of the second-mode vibration.

Figure 8 shows similar time histories for the optimally tuned passive system, i.e., $c = 1 \times 10^4$ N s/m and $f = 0$. Comparison of Figs. 7 and 8 reveals a much quicker damping of the first mode

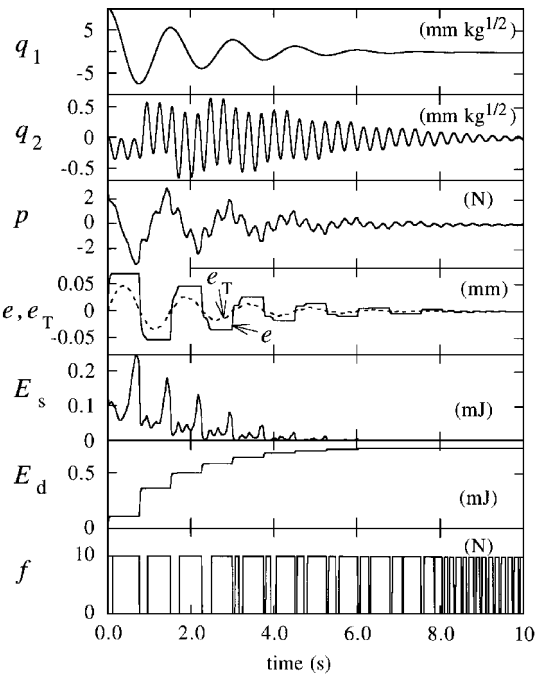

Fig. 7 Time history of vibration suppression by a system using the LQFC-1-b control law; single damper, only the first mode is excited by the initial condition, $c = 3 \times 10^3$ N s/m.

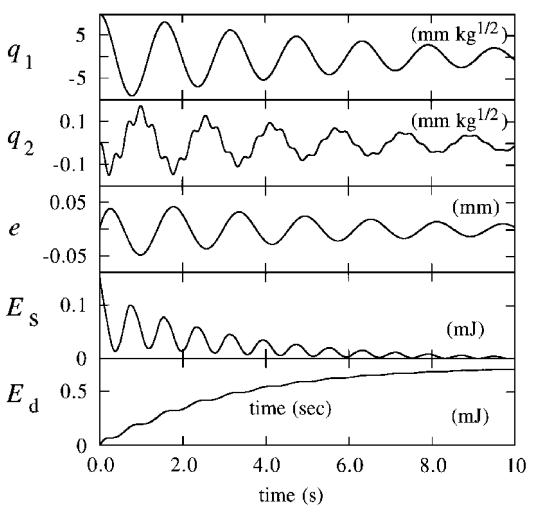

Fig. 8 Time history of free vibration decay of the optimally tuned passive system; single damper, only the first mode is excited by the initial condition, $c = 1 \times 10^4$ N s/m, $f = 0$.

in the semiactively controlled system than in the optimal passive system. The peaks of E_s are much higher in the initial phase in Fig. 7 than in Fig. 8 because e does not vary in Fig. 7, whereas f is kept high even when the absolute value of load on the damper, $|p|$, has been increased. In Fig. 7, the large amount of stored energy is dissipated in a short time. Figures 7 and 8 show that the semiactively controlled damper first stores a large amount of energy in itself and the truss member on which the damper is installed and subsequently dissipates the energy at a stroke, resulting in vibration being damped more quickly than in the passive system.

Vibration Suppression with Multiple Dampers

The preceding section showed that all of the semiactive approaches investigated are effective. To investigate whether these approaches are effective for suppressing multiple-mode vibration of the systems with multiple dampers and to investigate whether these approaches work nicely in combination with observers, further numerical investigation was performed by using the 10-bay truss with three variable dampers, shown in Fig. 5b. In this simulation

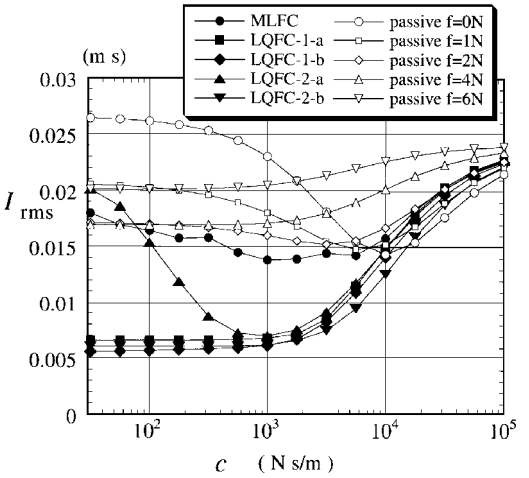

Fig. 9 Value of I_{rms} for systems using various semiactive control laws with observers and for passive systems with various levels of frictional force; three dampers, excited by an impulsive force at $t = 0$.

with three dampers, all of the vibration modes were taken into account by the mathematical model. For simplicity, all of the variable dampers were assumed to be identical, and c_i values of the dampers were assumed to be c. Similarly, all of the values of f_i in the passive system were assumed to be f. While the structure was still, a velocity of 0.1 m/s was given to the node shown in Fig. 5b by an impulsive force directed to $(1, 1, 0)$ in x–y–z coordinates, and the subsequent free vibration was suppressed according to the various control laws. The lowest five modes were taken into account to design the LQFC control laws, i.e., $n_c = 5$. In the design of LQFC control laws, the weighting matrices were set as indicated by Eqs. (31–33), and the r_2 value used was the same as that used in the preceding section.

For LQFC control laws, the state vector was estimated by the observer by using the output from the x and y directional displacement sensors mounted at the tip node shown in Fig. 5b. For the design of the observer, V_1 and V_2 were assumed as

$$V_1 = \bar{v}_1 \begin{bmatrix} 0 & 0 \\ 0 & I \end{bmatrix} \tag{35}$$

$$V_2 = \bar{v}_2 I \tag{36}$$

and $\bar{v}_1/\bar{v}_2$ was set to be 100 N^2 m^{-2} because this value was roughly optimal for many semiactive cases.

The values of I_{rms} obtained from the various approaches are shown in Fig. 9 as functions of c. Figure 9 shows that LQFC-1-a, LQFC-1-b, and LQFC-2-b with the observer give small value of I_{rms} and, thus, they work nicely in the structure with multiple dampers when c is less than 1×10^3 N s/m. As in the earlier cases, LQFC-2-a works nicely only when $c = 0.5$–1.0×10^3 N s/m. In this case, MLFC is not substantially effective.

Comparison with Active Vibration Suppression

To compare the performance and robustness of the semiactive approach with those of the active approach, we also designed and investigated a linear quadratic Gaussian (LQG) active control system. In this investigation of the active system, the e_i value of each variable damper was assumed to be directly controlled. This is equivalent to replacing the dampers with variable-length actuators whose axial stiffness is k_2. Then the equation of motion of the actively controlled truss is Eq. (6). As has been mentioned, the LQG control theory tells us that the optimal control law that minimizes the J value of Eq. (13) is given by Eqs. (14′) and (27). Also in this investigation, the values of R_1, R_2, V_1, and V_2 were assumed to be those given by Eqs. (31), (33), (35), and (36). Therefore, the resulting active control law design depended on the values of r_2 and $\bar{v}_1/\bar{v}_2$ used in the design.

In the numerical simulation, a velocity of 0.1 m/s was given to the node shown in Fig. 5b by an x-directional impulsive force when the structure was still, and the subsequent free vibration was suppressed according to the active control law. Because of the installation of actuators or dampers, the structural system was not symmetric with respect to the x–z plane. This impulsive force, therefore, excited not only the modes symmetric with respect to the plane but also the others. The sensor was assumed to measure only the x-directional displacement of the tip node shown in Fig. 5b, and the lowest three modes were actively controlled by using three actuators. For various values of $\bar{v}_1/\bar{v}_2$ and r_2, the active control law was designed, and the value of I'_{rms} from the active control law design was estimated by numerical simulation. The definition of I'_{rms} is given by Eq. (34), but in this case $\tau_I = 30$ s. Although the details are not shown, the results showed that there is in the $r_2 - \bar{v}_1/\bar{v}_2$ plane an optimal point that minimizes I'_{rms}. This was because of the effects of residual modes. The optimal point was approximately $\bar{v}_1/\bar{v}_2 = 50\,N^2\,m^{-2}$ and $r_2 = 3 \times 10^3$ kg, and the minimum value of I'_{rms} was 8.5×10^{-3} ms. The design of the active control law with these optimal values are referred to as LQG-1 in this paper.

On the other hand, the semiactive LQFC-1-b control law was also designed under the same conditions of sensors, locations of the dampers/actuators, and controlled modes as those under which the aforementioned active control was designed. This design of semiactive control law, which is referred to here as LQFC-1-b-1, gave $I'_{rms} = 8.9 \times 10^{-3}$ ms when $c = 10^2$ N s/m. This showed that, although the active control can suppress vibration better than the semiactive control can, the difference is very small in this example.

To compare the robustness of the semiactive and active approaches, the effects of dynamic characteristics variations on their performances were investigated. After the active and semiactive control laws were designed, the stiffnesses of the two-truss member (which are shown in Fig. 5b as truss member with stiffness uncertainty) were varied by the factor of $EA/EA_{nominal}$ keeping all of the parameters of the regulator and the observer unchanged, and the values of I'_{rms} were obtained by applying LQG-1 and LQFC-1-b-1. In the calculation, all of the modes were taken into account by the mathematical model. The results, together with those for the passive system whose dampers are optimally tuned for the nominal structure, are plotted in Fig. 10. The points plotted with filled symbols indicate that the system is unstable and, therefore, that the value of I'_{rms} will increase infinitely if the integration of Eq. (34) is performed for a long duration. Stiffness variation has relatively little effect on the performances of the passive system and the semiactive system LQFC-1-b-1. The performance of LQG-1, however, is very sensitive to the stiffness variation. The LQFC-1-b-1 system performs well even when LQG-1 results in a unstable system. This demonstrates that in this case the semiactive approach is much more robust than LQG.

In the preceding example, the natural frequencies of the six lowest modes are 0.651, 0.668, 3.19, 3.27, 3.54, and 7.47 Hz, and the three lowest modes are controlled. Therefore, this example may be

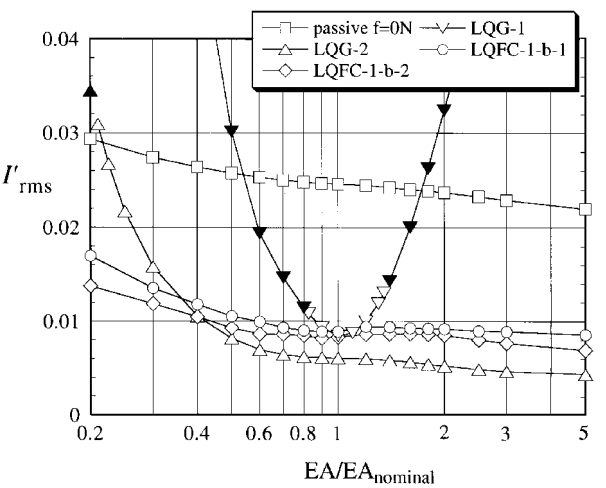

Fig. 10 Effect of stiffness variation of truss members on the performances of active, semiactive, and passive vibration suppression systems; LQFC-1-b-1, LQG-1: with one sensor, $n_c = 3$ and LQFC- 1-b-2, LQG-2: with two sensors, $n_c = 5$.

ill conditioned for LQG because there are residual modes whose natural frequencies are very close to that of a controlled mode. To investigate the robustness of LQG under better conditions, further investigation was performed by controlling the five lowest modes. Furthermore, the sensors were assumed to measure both the x- and y-directional displacements of the tip node. The values of r_2 and $\bar{v}_1/\bar{v}_2$ were set at 1×10^4 kg and 1×10^3 N^2 m^{-2}, respectively, such that the resulting I'_{rms} was roughly minimized. The resulting design is referred to as LQG-2. Similarly, an LQFC-1-b control law was also designed under the same condition of the sensors and controlled modes, and this control law design is referred to as LQFC-1-b-2. The value of r_2 and $\bar{v}_1/\bar{v}_2$ were the same as those of LQFC-1-b-1. As shown in Fig. 10, the performance of LQG-2 is substantially superior to that of LQFC-1-b-2 when the stiffness is the nominal value. Generally, LQG-2 is much more robust than LQG-1. It performs well and is robust when EA/EA_{nominal} is not very small. When the value of EA/EA_{nominal} is very small, however, LQG-2 is less robust and the system becomes unstable. Like LQFC-1-b-1, LQFC-1-b-2 is very robust although its performance is less than that of LQG-2 for the nominal structure.

Random Force Excitation

To learn whether the proposed semiactive schemes are effective for the suppression of random vibration, we also performed numerical simulations for the truss with three variable dampers excited by a random force. A random force directed to $(1, 1, 0)$ in the x–y–z coordinates was applied to the truss node shown in Fig. 5b. Its rms value was 0.1 N, and the power spectrum density was flat over the frequency range from 0.3 to 4.0 Hz and was zero in the rest of the frequency range, which covered the natural frequencies of the five lowest modes. Both the random force excitation and semiactive control started at time 0, and the rms displacement of the truss nodes was integrated from $t = 5$ to 35 s as a measure of performance I''_{rms}.

The values of I''_{rms} obtained from the various approaches are shown in Fig. 11 as functions of c. It is evident that LQFC-1-a, LQFC-1-b, and LQFC-2-b work well if c is less than 1×10^3 N s/m even when the truss is excited by a random force. As in the earlier case, LQFC-2-a works well only when c is between 6×10^3 and 3×10^4 N s/m, and MLFC is not substantially effective. Figure 11 shows that the semiactive vibration suppression is effective even when the structure is excited by a random force. When the value of c is less than 3×10^4 N s/m, the best performance is obtained by using LQFC-1-b.

In Fig. 11, the ratio of the minimum value of I''_{rms} for the passive system to that for the semiactive systems (except for MLFC) is about 1.5. This is much smaller than the corresponding ratio in Fig. 9, which is about 2.5. The reason for this smaller ratio is probably that, when the damping ratio of a system is ζ,

$$\int_0^\infty \delta_{\text{rms}}\, dt$$

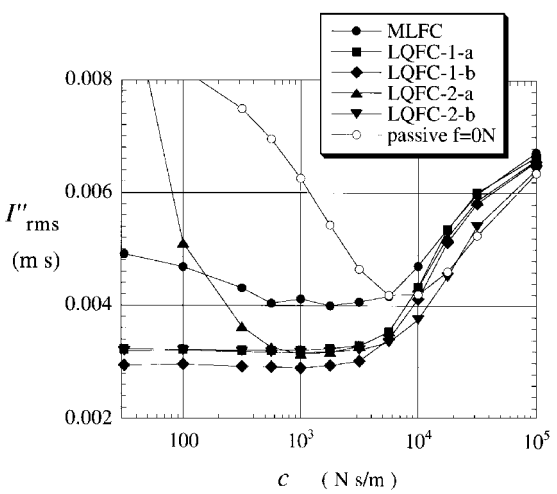

Fig. 11 Value of I''_{rms} for systems using various semiactive control laws and for a passive system, for forced random vibration; three dampers, with observers, two sensors, $n_c = 5$.

is proportional to ζ^{-1} for free decay vibrations and

$$\lim_{T\to\infty} \frac{1}{T} \int_0^T \delta_{\text{rms}}\, dt$$

is proportional to $\zeta^{-1/2}$ for vibrations excited by a steady random force. We can see that $(2.5)^{-1/2} = 1.58$ is very close to 1.5. Therefore, the small ratio in Fig. 11 does not indicate that the semiactive approach is less effective for the suppression of vibration induced by random excitation.

VI. Semiactive Vibration Suppression Experiments

Based on the simple mathematical model of the ER-fluid variable damper shown in Fig. 4, several control laws for semiactive vibration suppression have been proposed, and their performances have been numerically investigated in Sec. V. To see whether the semiactive approach is effective for an actual structure with an actual ER-fluid damper, we performed experiments using the 10-bay cantilevered beam truss shown in Fig. 5a. This is the same truss beam that was used for the numerical investigation in Sec. V except that 1) the tip mass and a center node were hung from 2.65-m-long wires (Fig. 5a) to compensate the effect of gravity and 2) two longitudinal truss members (Fig. 5a) were replaced with low-stiffness members to make the vibration frequency of the second mode a little closer to that of the first mode. The tensions of the tip and center wires were 50 and 130 N, respectively. The axial stiffness of the low-stiffness members are 5.1×10^3 N. Figure 5a also shows a block diagram of the experiment. Because the tip mass and the central node were hung from wires, the nodes could move in the x–z plane only.

In the experiment, the two lowest vibration modes in the x–z plane, whose frequencies were 0.67 and 2.63 Hz, were first excited by using a permanent magnet and a voice coil, and then the subsequent free vibrations of the two modes were suppressed semiactively by using the LQFC-1-b control law. The load on the variable damper p, the total elongation of the damper d, and the x-directional displacements of the tip mass u_1 and a node at the center of the beam u_2 were measured and fed to the processor as shown in Fig. 5a. The elongation and the displacement were measured by using noncontact eddy-current type and laser-beam type displacement sensors, respectively. The load was measured by using a strain-gauge type load cell. For the LQFC-1-b control law, the elongation e of the frictional element of the damper model, i.e., the elongation between points 2 and 4 of Fig. 4, needs to be known. Therefore, e was estimated as

$$e = d - p/k_1 \tag{37}$$

The modal displacements of the lowest two modes were estimated as

$$\hat{q}_1 = s_{11}u_1 + s_{12}u_2, \qquad \hat{q}_2 = s_{21}u_1 + s_{22}u_2 \tag{38}$$

where $\hat{q}_1$ and $\hat{q}_2$ are, respectively, the estimated values of the first and second modal displacements q_1 and q_2. Constants s_{ij} were selected such that $\hat{q}_1$ and $\hat{q}_2$ were affected by q_2 and q_1, respectively, as little as possible. Then, the LQFC-1-b control law given by Eqs. (18) and (14′) was implemented as follows in the terms of the measured variables:

$$V = 0$$

when

$$\{[1 + (k_2/k_1)]p - k_2 d\}\left(F_{1_{11}}\hat{q}_1 + F_{1_{12}}\hat{q}_2 + F_{1_{13}}\dot{\hat{q}}_1 + F_{1_{14}}\dot{\hat{q}}_2\right) < 0$$

$$V = V_{\max} \tag{39}$$

when

$$\{[1 + (k_2/k_1)]p - k_2 d\}\left(F_{1_{11}}\hat{q}_1 + F_{1_{12}}\hat{q}_2 + F_{1_{13}}\dot{\hat{q}}_1 + F_{1_{14}}\dot{\hat{q}}_2\right) > 0$$

where $F_{1_{ij}}$ is the ij element of the gain matrix given by Eq. (15). The cycle time for the processor to update the control signal was approximately 3 ms.

Figure 12 shows examples of the time histories obtained during the experiment. The values of e was estimated from Eqs. (37). The

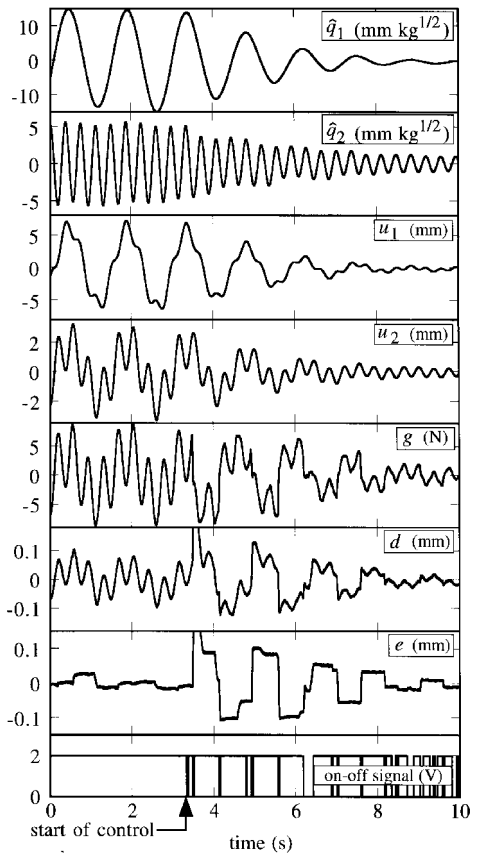

Fig. 12 Experimental time histories of semiactive suppression of multiple-mode vibration.

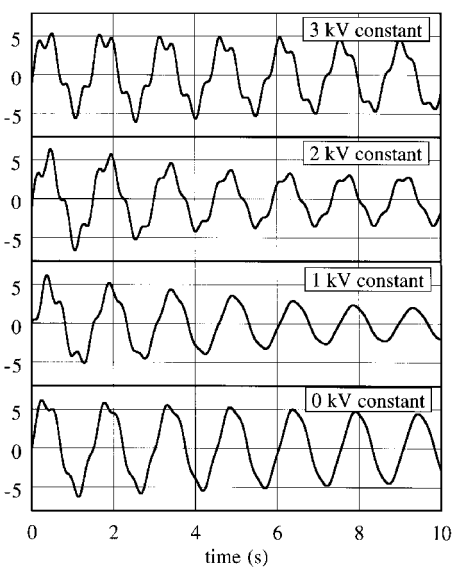

Fig. 13 Free decay multiple-mode vibration of the tip mass with constant input voltage.

variable g is the load at point 3 of the damper model shown in Fig. 4, which is given as

$$g = p - k_2 e \tag{40}$$

While the structure was vibrating freely, the control was started at $t = 3.3$ s, and the first-mode vibration was suppressed nicely in the subsequent 5 s. During this time, the variable damper was switched off near each peak of the first modal displacement. The tip-mass displacement u_1 was similarly reduced substantially. Although the damping rate of the second mode was slower than that of the first mode, the second mode also damped much more quickly than before the start of control. Figure 12 also shows that the amplitude

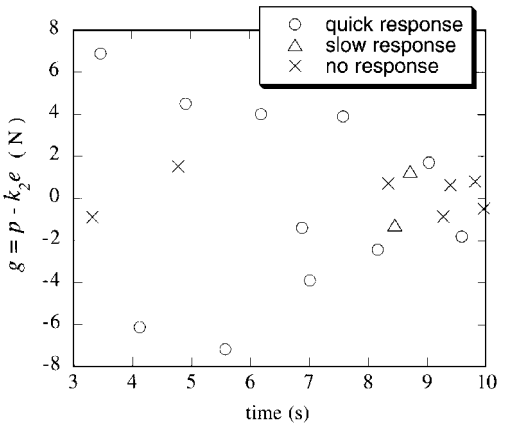

Fig. 14 Manner in which g responds to the switching off of the input voltage.

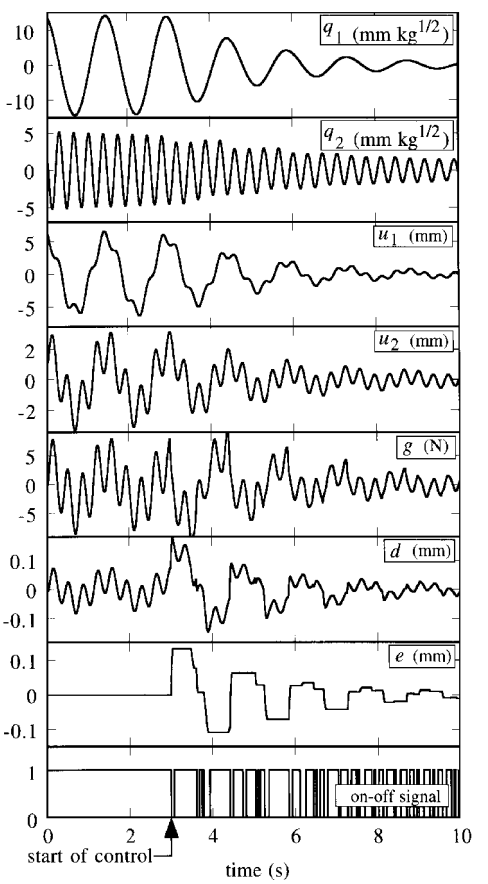

Fig. 15 Numerical simulation of semiactive vibration suppression experiment.

of the damper elongation d is much increased by the control action, resulting in the dissipation of more energy.

Figure 13 shows time histories of free vibration of the tip mass obtained while keeping the input voltage at various constant values. The damping in these time histories is very slow compared with that shown Fig. 12. These results of the experiment demonstrate that the present semiactive approach works nicely for damping the multiple-mode vibration of the actual structure.

After the start of control shown in Fig. 12, the controller switched off the input voltage 20 times. At most of these actions, the value of e varied stepwise, dissipating energy at the viscous element of the model shown in Fig. 4. Figure 14 shows the value of g at the moment of these actions, which value is derived from the data shown in Fig. 12. In Fig. 14, the response manner of e is classified into one of three groups: quick response, slow response, and no response. Figure 14 indicates that e does not respond to the switching off when the absolute value of g (which is the load on the frictional element

of the damper model of Fig. 4) is less than approximately 1 N. This suggests that $f_{\min}$ (which was estimated as 0.2 N in the extension test in Sec. II) could be as large as 1 N just after the application of high voltage, even when the voltage has been reduced to zero. Because e does not respond to the switching off when g is less than 1 N, the damping rate decreases when $t > 10$ s, by which time the vibration is suppresses to a low level. To suppress the vibration to a very small amplitude, a method to reduce the value of $f_{\min}$ has to be found.

Figure 15 shows results of numerically simulating the experiment under the assumption that $f_{\min} = 1.0$ N and the initial conditions are $q_1 = 14.4$ mm kg$^{1/2}$ and $q_2 = 5.2$ mm kg$^{1/2}$. The time histories are very similar to those shown in Fig. 12, even though the amplitude and phase of vibration are not exactly the same. This similarity indicates that the present modeling of the damper is acceptable for the design of schemes for the semiactive suppression of multiple-mode vibration.

VII. Concluding Remarks

A variable damper with ER fluid for semiactive control of the vibration of truss structures has been fabricated, and its characteristics have been measured. The characteristics of the damper are shown to be well modeled by a simple model composed of two springs, a viscous damping element, and a variable coulomb frictional element, whose frictional force is a monotonically increasing nonlinear function of the input voltage to the damper.

Based on the simple model of the variable damper, five on–off control laws for semiactive vibration suppression with the dampers have been proposed. Numerical simulation results show that all of them are effective for suppressing single-mode vibration but that only four of them are effective for suppressing the multiple-mode vibration of structures with multiple variable dampers. These control laws result in much quicker damping than that resulting from the use of an optimally tuned passive system. Semiactive vibration suppression has been shown to be much more robust than LQG active vibration suppression and to perform almost as well in an ill-conditioned case. Semiactive vibration suppression has also been shown to be effective not only for free vibration but also for forced vibration induced by a random excitation.

Semiactive vibration experiments have also been performed using a cantilevered truss beam and one of the proposed control laws. The experiments have demonstrated that the present semiactive control with the ER-fluid variable damper nicely suppresses multiple-mode vibration of an actual structure. Experimental results have shown general coincidence with numerical simulations, suggesting that the present modeling of the damper is appropriate.

This investigation has evaluated the performance of ER-fluid variable dampers stabilizing a truss structure, but it is clear that the proposed approaches and the results of the investigation are, in principle, applicable to all structural systems that have variable elements whose characteristics can be modeled as in Fig. 4.

References

[1] Balas, M. J., "Trends in Large Space Structure Control Theory: Fondest Hopes, Wildest Dreams," *IEEE Transactions on Automatic Control*, Vol. AC-27, No. 3, 1982, pp. 522–535.

[2] Balas, M. J., "Active Control of Flexible Systems," *Journal of Optimization Theory and Applications*, Vol. 25, No. 3, 1978, pp. 415–436.

[3] Onoda, J., Endo, T., Tamaoki, H., and Watanabe, N., "Vibration Suppression by Variable-Stiffness Members," *AIAA Journal*, Vol. 29, No. 6, 1991, pp. 977–983.

[4] Onoda, J., and Minesugi, K., "Alternative Control Logic for Type-II Variable-Stiffness System," *AIAA Journal*, Vol. 34, No. 1, 1996, pp. 207–209.

[5] Onoda, J., and Minesugi, K., "Semiactive Vibration Suppression of Truss Structures by Coulomb Friction," *Journal of Spacecraft and Rockets*, Vol. 31, No. 1, 1994, pp. 67–74.

[6] Onoda, J., Sano, T., and Kamiyama, K., "Active, Passive and Semiactive Vibration Suppression by Stiffness Variation," *AIAA Journal*, Vol. 30, No. 12, 1992, pp. 2922–2929.

[7] Onoda, J., and Minesugi, K., "Semiactive Vibration Suppression by Variable-Damping Members," *AIAA Journal*, Vol. 34, No. 2, 1996, pp. 355–361.

[8] Klass, D. L., and Martinek, T. W., "Electroviscous Fluids. I. Rheological Properties," *Journal of Applied Physics*, Vol. 28, No. 1, 1967, pp. 67–74.

[9] Stanway, R., Sproston, J. L., and Stevens, N. G., "Non-Linear Modeling of an Electro-Rheological Vibration Damper," *Journal of Electrostatics*, Vol. 20, No. 2, 1987, pp. 167–184.

[10] Gavin, H. P., Hanson, R. D., and Filisko, F. E., "Electrorheological Dampers, Part II: Testing and Modeling," *Journal of Applied Mechanics*, Vol. 63, Sept. 1996, pp. 676–682.

[11] Wang, K. W., Kim, Y. S., and Shea, D. B., "Structural Vibration Control Via Electro-Rheological-Fluid-Based Actuators with Adaptive Viscous and Frictional Damping," *Journal of Sound and Vibration*, Vol. 177, No. 2, 1994, pp. 227–237.

[12] Choi, S.-B., and Park, Y.-K., "Active Vibration Control of a Cantilevered Beam Containing an Electro-Rheological Fluid," *Journal of Sound and Vibration*, Vol. 172, No. 3, 1994, pp. 428–432.

[13] Onoda, J., Oh, H.-U., and Minesugi, K., "Semi-Active Vibration Suppression of Truss Structures by Electro-Rheological Fluid," 46th International Astronautical Federation Congress, IAF-95-I.4.07, Oslo, Norway, Oct. 1995.

[14] Kwakernaak, H., and Sivan, R., *Linear Optimal Control System*, Wiley-Interscience, New York, 1972.

A. Berman
Associate Editor